

# Organic functionalization on the non-ideal Si(001) surface – structure, bonding and reactivity

*Jan-Niclas Luy<sup>1,2</sup>, Ralf Tonner<sup>1,2\*</sup>*

<sup>1</sup>Fachbereich Chemie, Philipps-Universität Marburg, Hans-Meerwein-Straße 4, D-35032

Marburg

<sup>2</sup>Wilhelm-Ostwald-Institut für Physikalische und Theoretische Chemie, Universität Leipzig,

Linnéstraße 2, D-04103 Leipzig

## **ABSTRACT**

In this density functional theory study, the influence of the bonded dimer vacancy (DV) on the reactivity of the Si(001) surface is investigated. To this end, electronic and structural properties of the defect are analyzed. Band structure calculations reveal a higher-lying valence band which would suggest increased reactivity. However, the opposite is found when organic molecules for interface formation (acetylene, ethylene and cyclooctyne) are adsorbed at the defect. Significant reaction barriers have to be overcome in order to form bonds with defect atoms, while adsorption on the pristine surface is mostly direct. This suggests the presence of a, rather weak, Si-Si bond across the defect which must be dissociated before organic adsorbates can react. A rich adsorption and reaction network is found in addition to the structures known from the pristine surface. All three investigated adsorbates show different bonding characteristics. For acetylene and ethylene,

the preferred thermodynamic sink is the insertion into the defect, with the latter molecule even dissociating. Bulky cyclooctyne on the other hand avoids reaction with the defect due to steric demands imposed by the small defect cavity. The DV has no effect on reactivity of neighboring dimers. A combination of defect creation and hydrogen-precoverage could be a promising approach for selective surface functionalization. We thus show the influence of a non-ideal surface on organic functionalization and interface build-up reactions for a prototypical interface.

## INTRODUCTION

The (001) facet of silicon is one of the most studied surfaces in material science and technology due to its widespread use in electronic devices such as transistors, solar cells and LEDs. The desired electronic structure signatures defining the properties of the respective device often arise at the interface of silicon with other materials [1-3]. In recent years, particularly organic-silicon interfaces have sparked the interest of researchers due to combining advantages of the mature silicon-based technology with the chemical richness of organic compounds [4-6].

However, the high reactivity of the pristine Si(001) surface (Figure 1a) makes creating well-defined interfaces challenging [7]. To address this issue, first a contact layer has to be synthesized from selective reactions between surface dimers and suitable organic molecules which saturate reactive dangling bonds. As a promising approach, 1,3-dipolar [8] and [2+2] [9, 10] cycloadditions have been identified (Figure 1e). Cyclooctyne (Figure 1b) has been found to be an excellent platform molecule [9, 10]. When the adsorption is done with bifunctional anchor molecules, such as ethynyl-cyclopropyl-cyclooctyne [11] or methyl enolether functionalized cyclooctyne [12], additional organic layers can be grown on the first layer [13].

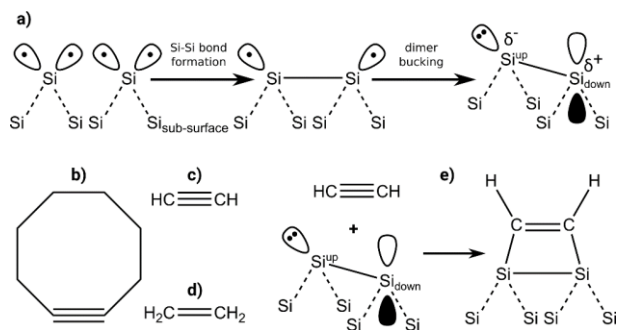


**Figure 1.** a) Reconstruction of the Si(001) surface into dimers which can well be described with a lone-pair at  $\text{Si}_{\text{up}}$  and an empty p-orbital at  $\text{Si}_{\text{down}}$ . b) Cyclooctyne, c) acetylene and d) ethylene as investigated in this work. e) Example of a [2+2]-type reaction with a silicon surface dimer.

Up to now, most of the work on organic thin-layer growth on semiconductor surfaces has focused on pristine substrates while some studies considered step edges [14, 15]. This is possible since substrate preparation techniques that suppress defect formation effectively under UHV conditions exist [16]. However, we believe that defects, despite their unfavorable reputation, could actually be used to increase the selectivity of surface reactions and offer a new path to precise patterning [17, 18]. Indeed, in a similar spirit, hydrogen-precovered surfaces with distorted dangling bond configurations have been shown to exhibit an increased reactivity in the case of ethylene adsorption on Si(001) [19, 20]. The main motivation of the present work is therefore to quantify and understand the changes in reactivity of defects with respect to the pristine surface. Furthermore, the investigation of non-ideal surfaces will help to create more realistic computational models of organic-inorganic interfaces.

In the past, acetylene and ethylene (Fig. 1c,d) have been computationally studied as simple models for cycloaddition reactions of unsaturated hydrocarbons on the pristine Si(001) $c(4\times 2)$  surface by us and others [20, 21]. In the case of ethylene, there exists a  $\pi$ -complex-like precursor bound to a  $\text{Si}_{\text{down}}$  atom preceding covalent attachment in a [2+2]-like fashion [22]. For acetylene,

adsorption is direct and the  $\pi$ -complex instead serves as a transition state (TS) between two *sub-surface* modes [23]. Notably, experiment indicates an indirect adsorption path via a precursor state which has been discussed by us before [23, 24]. Both acetylene and ethylene adsorb preferentially *on-top* a single dimer or *bridged* between two dimers [25]. The already mentioned cyclooctyne (Figure 1b) [26] is the smallest stable cyclic alkyne and contains a ring strain energy (RSE) of about 80 kJ/mol [13]. Reactions involving the triple bond partly release this RSE which increases selectivity and makes catalysts obsolete [27]. Due to this benefit, cyclooctyne and its derivatives are considered promising candidates for layer-by-layer interface building schemes [28].

Defect-containing surfaces should show a richer adsorption chemistry due to the presence of additional structural motives. In order to focus the scope of this study, we omit defects of higher dimensionality and limit the investigation to the thermodynamically most favorable intrinsic point defect, the *bonded dimer vacancy* (DV) [29]. In comparison to the DV (Figure 2c), single atom vacancies are 94-98 kJ/mol (Figure 2a,b) less stable. This value is in good agreement with earlier results [30] and experiments showing a high DV concentration of 9% for a surface cleaved at 0.4° and annealed at 800 °C [31]. Moving a whole Si dimer into an *ad*-position requires just 33 kJ/mol (Figure 2f) per atom which is even less compared to creating an *ad-atom* (68 kJ/mol, Figure 2e). This value aligns well with a study where strong diffusion of *ad-dimers* on Si(001) was found [32]. The related *twisted dimer vacancy* reconstruction (Figure 2d) shows larger bond distances and requires 45 kJ/mol per atom to form. This result agrees with tight binding calculations reported earlier [33]. Additionally, it was proposed that the DV is the energetic sink for bulk vacancies as they slowly diffuse to the surface [34].

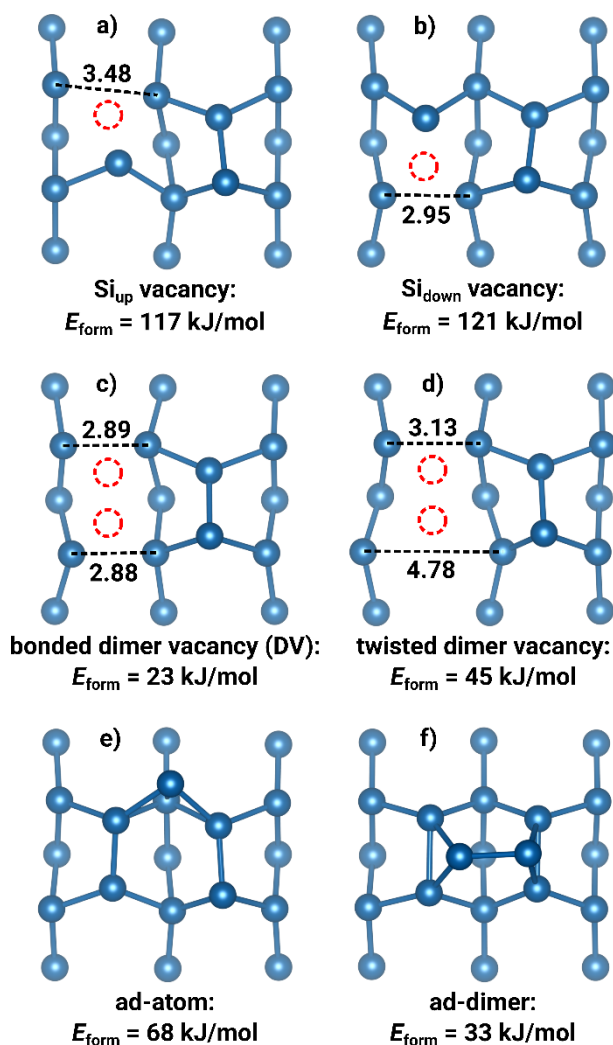


**Figure 2.** Most common intrinsic point defects of Si(001) as considered in this study. Bond lengths are given in Å. Defect formation energies ( $E_{\text{form}}$ ) are calculated per atom with respect to the cohesive energy of bulk Si ( $E_{\text{coh}} = -553$  kJ/mol, see Equation (2)). Our values agree well with earlier results [35]. Vacancies are indicated by red circles.

We note in passing that in many scanning tunneling microscopy (STM) studies the DV has also been referred to as “A-defect” [36] while distinguishing it from the double-DV (“B-defect”) and dissociatively adsorbed water molecules (“C-defect” [37]). However, the identification of different

defects has not been unambiguous in the past since water molecules produce similar STM features to missing atom defects in a large range of bias voltages [38].

The results section is divided into four parts. First, the atomic and electronic structure of the DV is discussed taking bond parameters and formation energies into account. In the second part, the thermodynamic features of molecular adsorption is investigated. Bonding analysis is performed in the third part. Lastly, the kinetic influence of the DV on adsorption is discussed with the help of reaction networks.

## **METHODS**

Density functional theory (DFT) calculations were performed with the Vienna Ab initio Simulation Package (VASP 5.4.4 [39-41]). The generalized gradient approximation-(GGA)-based exchange-correlation functional proposed by Perdew, Burke and Ernzerhof (PBE) [42] was used in conjunction with the projector-augmented wave (PAW) method using the “standard” pseudo potentials for all atoms (version PBE5.4) [43]. Dispersion effects were treated with the DFT-D3 scheme using the “Becke-Johnson”-type damping function [44, 45]. The precision tag was set to accurate and a total energy difference of at most  $10^{-5}$  eV was used for SCF convergence, while setting the plane wave energy cutoff to 400 eV. For structure optimization, the force convergence criterion was  $10^{-2}$  eV/Å. The surface was modelled with a six-layered slab-supercell in periodic boundary conditions. The theoretical lattice parameter ( $a = 5.418$  Å) was determined previously [9]. The bottom side of the slab was saturated with two hydrogen atoms per Si at the Silane ( $\text{SiH}_4$ ) bond length (1.480 Å) [46] while the bottom two Si-layers are frozen at their bulk positions. The thickness of the vacuum layer between periodically repeated slabs was at least 13 Å. Electronic levels around the Fermi-energy are smeared out by  $\sigma = 0.05$  eV with Gaussian functions to

accelerate self-consistent field convergence. Momentum space was sampled by a  $1 \times 2$   $\Gamma$ -centered  $k$ -point mesh. This computational setup has yielded accurate results for adsorbates on the pristine surface in the past [9]. Reaction paths have been calculated with the climbing-image nudged elastic band (CI-NEB) [47] method. Transition states found were further optimized with the dimer method [48]. In addition, the influence of spin-polarization on the wave function of the DV was investigated: Starting the SCF procedure with a magnetization at the four defect atoms (antiferromagnetic configuration), the calculation converged to the same values as for the non-polarized case. We thus present the latter throughout the manuscript.

Crystal orbitals and energy decomposition analysis for extended systems (pEDA) [49] were calculated with ADF-BAND [50] version 2019.301 except in Figure 4 where version 2019.105 was used. Again, the PBE-D3(BJ) functional was used in conjunction with the atom centered TZ2P [51] basis set. Scalar relativistic effects were treated with the zeroth order regular approximation (ZORA) [52]. The pEDA method decomposes the bond energy ( $\Delta E_{\text{bond}}$ ) between two fragments A and B into well-defined quantities allowing for a chemically meaningful interpretation. The bond energy ( $\Delta E_{\text{bond}}$ ), or negative dissociation energy, is the sum of the interaction energy ( $\Delta E_{\text{int}}$ ) and a preparation energy ( $\Delta E_{\text{prep}}$ ), which is defined as the difference between the isolated fragments and the states found in the final complex.  $\Delta E_{\text{int}}$  can be further divided into an empirical dispersion term ( $\Delta E_{\text{disp}}$ ) and an electronic term ( $\Delta E_{\text{elec}}$ ). The actual pEDA procedure then decomposes  $\Delta E_{\text{elec}}$  into a quasiclassical electrostatic contribution ( $\Delta E_{\text{elstat}}$ ), the Pauli repulsion term ( $\Delta E_{\text{Pauli}}$ ) obtained by antisymmetrizing and normalizing the fragment wave functions and finally an orbital interaction ( $\Delta E_{\text{orb}}$ ) that results from relaxing the intermediate wave function and includes charge transfer and polarization effects (equation (1)).

$$\Delta E_{\text{elec}} = \Delta E_{\text{Pauli}} + \Delta E_{\text{elstat}} + \Delta E_{\text{orb}} \quad (1)$$

The orbital term can be further dissected by the Natural Orbitals for Chemical Valence (NOCV) scheme. Here, the NOCVs  $\Psi_i$  are constructed as eigenvectors that diagonalize the deformation density matrix in the basis of fragment orbitals. The electron density difference  $\Delta\rho_{\text{orb}} = \rho_{\text{AB}} - \rho^0$  is then expressed by deformation densities  $\sum \rho_i$  which aid in visual characterization of the bond. Corresponding eigenvalues  $v_i$  quantify the amount of charge transferred between NOCVs.

### *Thermodynamic corrections*

Calculation of vibrational modes needed for thermodynamic corrections become prohibitively expensive for large simulation cells. Therefore, we devised a scheme that allows  $\Delta G_{\text{ads}}$  values to be determined approximately by considering only a subsection of the Hessian matrix. In the simplest case, only adsorbate atoms are displaced in the finite-differences method implemented in VASP. Convergence of  $\Delta G_{\text{ads}}$  is then achieved by including ever larger nearest neighbor or next-nearest neighbor spheres in the surface. During calculation of the dynamical matrix, atoms outside of the considered sphere are kept fixed. This approach yields accurate results for the adsorption free energy of acetylene (this work: 69 kJ/mol, full Hessian [15]: 68 kJ/mol, at 300 K) and is expected to also perform well for larger adsorbates as long as all important Hessian elements are calculated. Benchmarking of this approach, further details and a python script allowing parallel computation can be found in the in the supporting information (Table S1).

### *Convergence of cell parameters*

In order to investigate an isolated defect as it would be present on an actual surface, the number of primitive unit cells along directions  $x$  and  $y$  have to be chosen such that electronic levels are sufficiently localized and artificial interactions with periodic images avoided. In addition, the

structural strain introduced by a defect has to decay within the super cell. Thus, to converge the formation energy ( $E_{\text{form}}$ ) of a DV defect, slabs of different sizes were generated and compared in Table 1.  $E_{\text{form}}$  is calculated as the difference of the total energy of the pristine slab ( $E_{\text{pristine}}$ ) and the defect containing slab ( $E_{\text{defect}}$ ) normalized to the number of defect atoms  $N$  (i.e. 2 for the DV) which is added to the cohesive energy  $E_{\text{coh}}$  of Si in the diamond structure (equation (2)).

$$E_{\text{form}} = E_{\text{coh}} + (E_{\text{defect}} - E_{\text{pristine}})/N \quad (2)$$

The error ( $\Delta E_{\text{form}}$ ) is with 18 kJ/mol largest for the smallest six-layered slab of a 4×4 supercell. Addition of another layer lowers the penalty by 4 kJ/mol while an eighth layer converges it to within 2 kJ/mol. Doubling the size of the slab along rows of surface dimers leading to a 8×4 supercell lowers the penalty by 11 kJ/mol regardless of the layer number. Doubling the slab also along the second direction (8×8 supercell) has no significant impact on defect formation energies. The band gap converges slightly faster with just one additional layer. Thus, it can be concluded that slabs used for studying defects should contain a larger number of layers and unit cells than for pristine surfaces. All calculations in this study are therefore performed in the 8×4 supercell with 8 layers where 1/16th of dimers are missing (see Figure S1 in the supporting information for a plot of the atomic structure).

**Table 1.** Errors in formation energy ( $\Delta E_{\text{form}}$ ) and error in bandgap ( $\Delta E_{\text{Gap}}$ ) with respect to the largest cell investigated in kJ/mol.

Supercell	No. of layers	$\Delta E_{\text{form}}$	$\Delta E_{\text{Gap}}$
4×4	6	18	18
4×4	7	14	23
4×4	8	12	23

8×4	6	7	17
8×4	7	3	22
8×4	8	< 1	22
8×8	8	0	21

---

## RESULTS AND DISCUSSION

### *Energy of formation and atomic structure of the DV defect*

First, we will discuss the structural changes induced by the DV defect. Removal of a dimer from the pristine surface creates four new dangling bonds at former *sub-surface* atoms (see Figure 3c). Thus, the sum of reactive sites should increase by two, making the surface more reactive. However, as we will see, this is not the case. Instead, the defect relaxes into a more favorable configuration by forming single-bonds across the defect. Structural support for this relaxation model is given by a rather short Si-Si distance of 2.88 Å ( $d(\text{Si-Si})$  in bulk-like layer = 3.83 Å) as well as noticeable displacement of neighboring atoms from their position on the pristine surface (Figure 3c). The bond is 0.5 Å longer than a Si-Si-bond in the bulk (2.35 Å) due to constraints imparted by the lattice but significantly shorter than the sum of van-der-Waals radii (4.20 Å [53]). In order to enable the formation of two short Si-Si bonds found in the defect, one dimer adjacent to the DV flips (Figure 3b) thus breaking the buckling periodicity of the  $c(4\times 2)$  reconstruction.

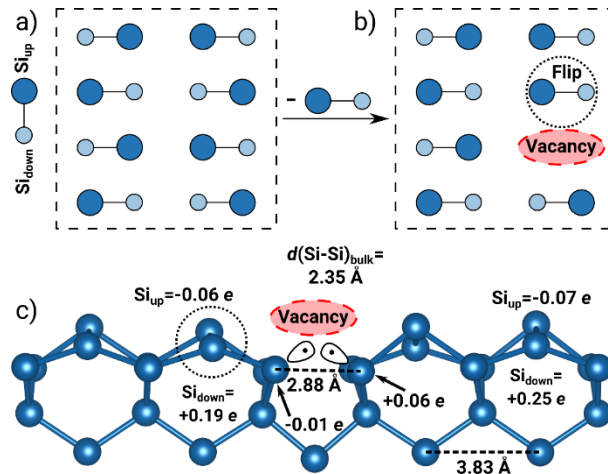


**Figure 3.** (a) Top view of a pristine  $4 \times 4$  supercell of the Si(001) surface showing only dimers.  $\text{Si}_{\text{down}}$  atoms are represented by small circles,  $\text{Si}_{\text{up}}$  atoms by larger circles. (b) Removal of a dimer results in the formation of a DV (red oval) and the flipping (black circle) of a neighboring dimer. (c) Side view of the bonded DV with structural and electronic properties. Dashed lines: Si-Si distances. Atomic partial charges are given in elementary charge units  $e$ .

#### *Electronic structure of the DV defect*

Next, the electronic structure of the DV (Figure 4) in reciprocal (band structure) and real (crystal orbitals (CO)) space is compared to the pristine surface.

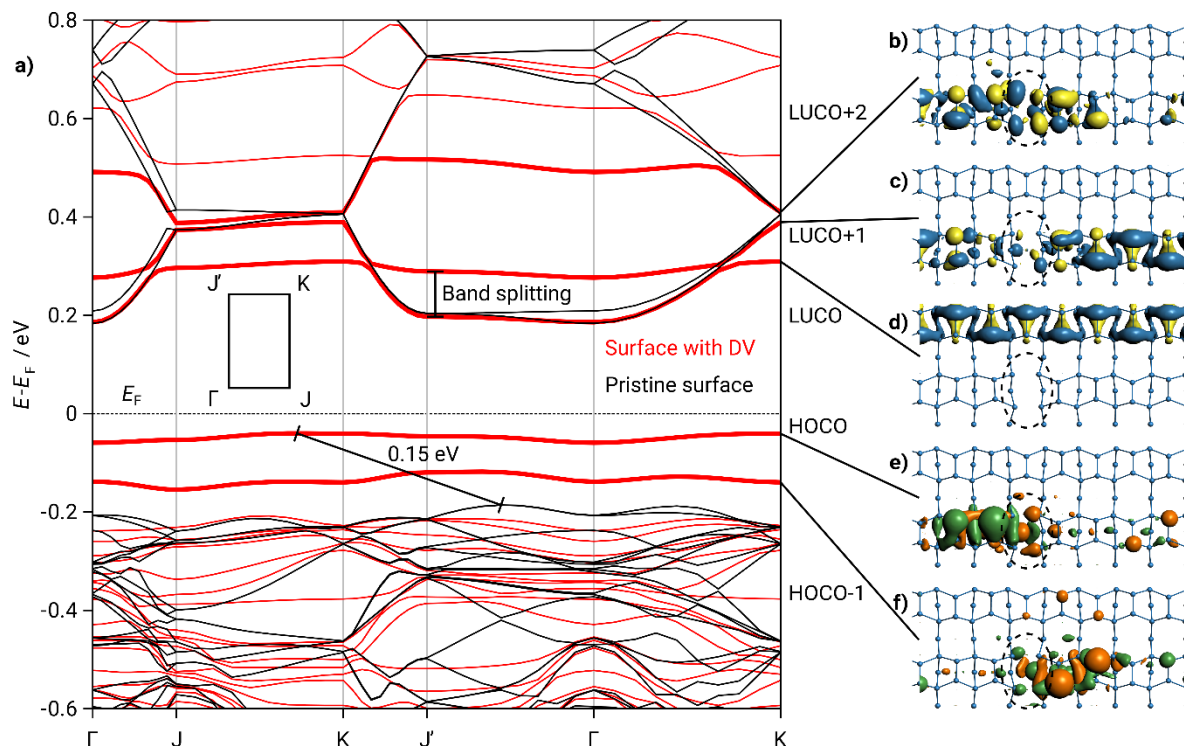


**Figure 4.** a) Band structure of the pristine (black) and DV-including (red)  $8 \times 4$  surface supercell. Energies are given with respect to the Fermi energy ( $E_F$ ) of the pristine surface. The surface bands stemming from the DV are aligned to match the lowest calculated band of pristine surface at the  $\Gamma$ -point. Additional bands introduced by the defect close to the Fermi edge are emphasized in bold and the reduction of the band gap is indicated by a flat-headed arrow. The position of high-symmetry points in the surface unit mesh is shown as an inset. b-f) Selected crystal orbital plots at the  $\Gamma$ -point. The position of the defect is indicated with a dashed oval.

With introduction of the defect, two bands (bold red) are elevated into the former band gap, thus narrowing the gap by about 0.15 eV. The valence bands are strongly localized as indicated by the absence of band dispersion and shown by real space plots of the highest occupied COs: HOCO and HOCO-1 at the  $\Gamma$ -Point (Figure 4e,f). Conversely, on the pristine surface the HOCO is doubly degenerate and delocalized over the whole cell (Figure S2) as indicated by strong band dispersion.

Furthermore, these plots reveal hybridization between defect orbitals and  $\text{Si}_{\text{up}}$  lone pairs with quickly decaying spatial extent. Degeneracy between both sides of the defect is lifted by breaking of translational symmetry in this supercell model. Thus, an energetic separation of the formerly degenerate HOCO and HOCO-1 is found. Interaction of the DV with the flipped dimer (black circle Figure 3) is slightly less favorable than interaction with alternating dimers, probably due to  $\text{Si}_{\text{up}}$  lone pair repulsion in the HOCO (large green lobes). In the lowest unoccupied bands, hybridization between the DV and empty p-orbitals of  $\text{Si}_{\text{down}}$  atoms is observed (LUCO+1, LUCO+2). As in the occupied bands, this results in slightly reduced dispersion and more localized orbitals compared to the LUCO of the pristine surface. The conduction band minimum is found at the  $\Gamma$ -point. There and at all other high-symmetry points, the presence of the defect causes splitting of formerly degenerate bands. In addition, avoided crossings appear along Brillouin zone paths propagating in x-direction (e.g.  $\Gamma$ -J) as a result of translational symmetry breaking. Therefore, electron mobility along the x-direction is expected to be reduced. Notably, there is good qualitative agreement between the band structure of the DV and earlier work on the stepped Si(001) surface [54].

Due to the LUCO+1 showing almost no electron density at the flipped dimer and a lower positive charge at its  $\text{Si}_{\text{down}}$  atom, Lewis-acidity should decrease. This finding is corroborated by Natural Population Analysis which reveals that the four defect atoms carry a partial charge that is opposite to their neighboring dimer atoms (black arrows in Figure 3). The magnitude of the charge ( $-0.01$  to  $+0.06 e$ ) is smaller than at the  $\text{Si}_{\text{down}}$  atom (up to  $+0.25 e$ ) which should result in decreased electrophilicity. This is indeed the case as shown in the next section.

### *Reactions with small unsaturated hydrocarbons*

The Lewis acidity of the flipped  $\text{Si}_{\text{down}}$  atom can be estimated by calculating its bonding energy with a Lewis donor. Here, we chose ethylene since the system has been intensively analyzed for the pristine surface [22]. With the help of the energy decomposition analysis for extended systems (pEDA), we can quantify the Lewis acidity (Table S2). The interaction energy (which considers the preparation energy to deform the fragments for bonding) is much lower for the flipped dimer ( $\Delta E_{\text{int}} = -71$  kJ/mol) compared to a dimer on the pristine surface ( $\Delta E_{\text{int}} = -113$  kJ/mol) leading to a reduction in bonding energy from -82 kJ/mol to -56 kJ/mol. The nature of the bonding is similar – as indicated by the pEDA contributions showing similar trends – but the total bonding energy and thus the Lewis acidity of the flipped dimer is considerably reduced. The Lewis basicity of the  $\text{Si}_{\text{up}}$  atom is hardly changed as shown by the interaction with a Lewis acid ( $\text{BH}_3$ , Table S2) even though the HOCO energy changes.

Understanding the reactivity at the DV site is a prerequisite for the understanding of organic functionalization on the surface. Thus, the adsorption of interface building block cyclooctyne and its model molecules acetylene and ethylene are investigated. We find four thermodynamically favorable adsorption modes which are presented in Figure 5. Of those, only the ‘*on-top*’ mode (1) also exists on the pristine surface (a further adsorption mode bridging two dimers is not investigated here since it is less stable at low coverages [21]). Unique to the DV are the modes ‘*pedestal*’ (2), ‘*side-on*’ (3) and ‘*bridge*’ (4). The *pedestal* mode cures the defect by forming four C-Si bonds, effectively replacing the missing Si dimer. The *side-on* mode is created by reaction with one dimer and one defect atom. Hence, four adsorbent molecules would be needed to cure the defect. Lastly, the *bridge* mode connects two opposing defect atoms, requiring two molecules to cure the defect.

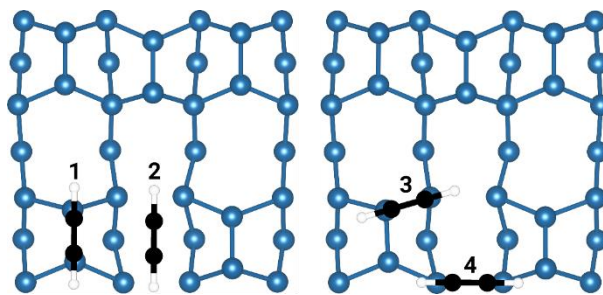


**Figure 5.** Adsorption modes onto the defect are shown representatively for acetylene: **1** *on-top*, **2** *pedestal*, **3** *side-on* and **4** *bridge*. Shown are the first three layers of a Si(001) slab with a DV.

**Table 2.** Bonding energies of acetylene, ethylene and cyclooctyne in different adsorption modes at a DV.<sup>a</sup>

Mode	Acetylene	Cyclooctyne	Ethylene
<i>On-top</i> (pristine)	-266	-305	-200
<i>On-top</i>	-268	-307	-200
<i>Pedestal</i>	-302	-250	-321 <sup>b</sup>
<i>Side-on</i>	-229	-261	-167
<i>Bridge</i>	-281	-273	-203

<sup>a</sup> All energies in kJ/mol computed with PBE-D3(BJ)/PAW. The bonding energy  $\Delta E_{\text{bond}}$  is negative by convention for stable modes and calculated as the difference between isolated reactants and products.

<sup>b</sup> The C=C bond dissociates (see Figure 8).

Bonding energies of the three molecules are listed in Table 2. Interestingly, the energy in the *on-top* mode is unchanged with respect to the pristine surface. However, there is large variation in the values of the other modes.

In the case of acetylene, *bridge* shows only slightly stronger bonding (-281 kJ/mol) than *on-top* (-268 kJ/mol) while it is weakest for *side-on* (-229 kJ/mol). The *pedestal* mode shows the strongest bond with -302 kJ/mol although the carbon-carbon triple bond is reduced to a single bond. These data suggests that a thermodynamic driving force of at least 20 kJ/mol exists in favor of *pedestal* which is desirable for selective surface functionalization. This beneficial defect property might be used in a combined approach with hydrogen pre-coverage of Si(001) (Figure S3). Here, the *pedestal* mode is further stabilized by -15 kJ/mol while *bridge* is destabilized by 4 kJ/mol and *side-on* is entirely blocked. Furthermore, H<sub>2</sub> reacts preferentially with dimer atoms ( $E_{\text{bond}}(\textit{on-top}) = -166$  kJ/mol) over defect atoms ( $E_{\text{bond}}(\textit{pedestal}) = -85$  kJ/mol) leaving the latter intact for reactions with unsaturated hydrocarbons.

For cyclooctyne, two conformers (tilt towards and tilt away from the DV) are found in the *on-top* mode (only the more stable one is listed in Table 2). While those conformers are separated energetically by just 3 kJ/mol, dispersion-induced bending [9] away from the defect is pronounced and the adsorption height is reduced by 0.262 Å (see Figure S4 for the tilt away-conformer). This might allow a steering effect on adsorption of further cyclooctyne molecules on specific adsorption sites as observed on the pristine surface [55]. While adsorption into *on-top* is -39 kJ/mol more favorable when compared to acetylene, this trend is less pronounced for *side-on* (-32 kJ/mol) and even reversed for *bridge* (8 kJ/mol) and *pedestal* (52 kJ/mol). In order to explain this observation, a detailed bonding analysis by pEDA is performed in the next sub-section.

Most trends observed above for acetylene are also found for ethylene. However, this molecule shows adsorption energies which are 60-80 kJ/mol smaller. The weakest bond is formed in the *side-on* mode (-167 kJ/mol) followed by *on-top* (-200 kJ/mol) and *bridge* (-203 kJ/mol). Again, the *pedestal* mode (-321 kJ/mol) presents an exception as the former C=C is cleaved in order to

form two CH<sub>2</sub> fragments (see Figure 8). The resulting structure is similar to the adsorption of SiH<sub>x</sub> molecules at the DV as calculated by tight binding approaches [56].

### *Bonding analysis*

In order to explain the trends in the adsorption energies of Table 2, pEDA calculations are performed as summarized in Table 3. The pEDA is a powerful method that decomposes the interaction energy between two molecular fragments into chemically meaningful quantities such as quasiclassical electrostatic interactions ( $\Delta E_{\text{elstat}}$ ), orbital interaction ( $\Delta E_{\text{orb}}$ ) and Pauli repulsion ( $\Delta E_{\text{Pauli}}$ ). The total bonding energy is obtained by subtracting the preparation energy (deformation, electronic excitation) of the fragments. Further details of the pEDA are found in the methods section.

### *On-top*

Cyclooctyne and acetylene show almost identical adsorption energies in the *on-top* mode at the DV and on the pristine surface (Table 4). This observation also holds true for most pEDA terms with the exception of the Pauli repulsion which is slightly more positive at the DV. However, this is exactly counterbalanced by a stronger orbital interaction term. We can thus conclude that the dimer neighboring a DV defect shows the same reactivity as on the pristine surface.

The 39 kJ/mol larger bonding energy of cyclooctyne when compared to acetylene can be explained by a release of 53 kJ/mol RSE (manifested through a reduced preparation energy,  $\Delta E_{\text{prep}}$ ) together with increased dispersion interaction ( $\Delta \Delta E_{\text{int}}(\text{disp}) = -24$  kJ/mol).

**Table 3.** pEDA results for acetylene and cyclooctyne in the *pedestal* and *on-top* modes. All energies in kJ/mol at PBE-D3(BJ)/TZ2P computed at the  $\Gamma$ -point.

	<i>pedestal</i> <sup>a</sup>					<i>on-top</i> <sup>b</sup>					<i>side-on</i> <sup>b</sup>		<i>sub-surface</i> [23]		
	acetylene		cyclooctyne		$\Delta\Delta E$	acetylene		cyclooctyne		$\Delta\Delta E$	acetylene			$\Delta\Delta E$	
	kJ/mol	%	kJ/mol	%		kJ/mol	%	kJ/mol	%		kJ/mol	%	kJ/mol	%	
$\Delta E_{\text{int}}$	-1165		-1079		86	-664		-649		15	-720		-656		-64
$\Delta E_{\text{int}}(\text{disp})^c$	-9	1	-63	6	-54	-10	2	-34	5	-24	-21	3	-22	3	+1
$\Delta E_{\text{int}}(\text{elec})^c$	-1156	99	-1016	94	140	-654	98	-615	95	39	-699	97	-634	97	-65
$\Delta E_{\text{Pauli}}$	2966		3121		155	1354		1492		138	1796		1587		209
$\Delta E_{\text{elstat}}^d$	-1649	40	-1754	42	-105	-834	42	-938	45	-104	-1005	40	-912	41	-93
$\Delta E_{\text{orb}}^d$	-2473	60	-2383	58	90	-1176	58	-1169	55	7	-1489	60	-1310	59	-179
$\Delta E_{\text{prep}}$	862		825		-37	391		339		-53	487		520		-33
$\Delta E_{\text{prep}}(\text{M})^e$	707		664		-43	365		312		-53	368		364		+4
$\Delta E_{\text{prep}}(\text{S})^e$	156		161		5	27		27		0	119		156		-37
$\Delta E_{\text{bond}}$	-303		-255		48	-273		-310		-37	-233		-136		-97
$\Delta E_{\text{bond}}(\text{PAW})^f$	-302		-250		52	-268		-307		-39	-229		-120		-109
$d(\text{C-C}) / \text{\AA}$	1.632		1.657			1.356		1.367			1.350		1.348		

<sup>a</sup> Fragments are generated from homolytic cleavage at C-Si into neutral quintuplets.

<sup>b</sup> Fragments are generated from homolytic cleavage at C-Si into neutral triplets.

<sup>c</sup> Percentage values: Relative contributions of dispersion and electronic effects to the interaction energy  $\Delta E_{\text{int}}$ .

<sup>d</sup> Percentage values: Relative contributions of the attractive pEDA terms  $\Delta E_{\text{elstat}}$  and  $\Delta E_{\text{orb}}$ .

<sup>e</sup> Preparation energies of the molecule (M) and substrate (S) contain structural contributions and electronic excitations.

<sup>f</sup> Deviations with respect to the PAW result are due to the basis set and simulation cell set-up differences.

**Table 4.** pEDA results for acetylene and cyclooctyne in the *on-top* mode at the pristine surface.All energies in kJ/mol at PBE-D3(BJ)/TZ2P computed at the  $\Gamma$ -point.

<i>on-top</i> (pristine) [9] <sup>a</sup>				
	acetylene		cyclooctyne	
	kJ/mol	%	kJ/mol	%
$\Delta E_{\text{int}}$	-668		-658	
$\Delta E_{\text{int}}(\text{disp})$ <sup>b</sup>	-12	2	-43	7
$\Delta E_{\text{int}}(\text{elec})$ <sup>b</sup>	-656	98	-615	93
$\Delta E_{\text{Pauli}}$	1323		1468	
$\Delta E_{\text{elstat}}$ <sup>c</sup>	-828	42	-936	45
$\Delta E_{\text{orb}}$ <sup>c</sup>	-1152	58	-1148	55
$\Delta E_{\text{prep}}$	389		339	
$\Delta E_{\text{prep}}(\text{M})$ <sup>d</sup>	364		313	
$\Delta E_{\text{prep}}(\text{S})$ <sup>d</sup>	25		26	
$\Delta E_{\text{bond}}$	-279		-319	
$\Delta E_{\text{bond}}(\text{PAW})$ <sup>e</sup>	-268		-308	
$d(\text{C-C}) / \text{\AA}$	1.357			

<sup>a</sup> Fragments are generated from homolytic cleavage at C-Si into neutral triplets.<sup>b</sup> Percentage values: Relative contributions of dispersion and electronic effects to the interaction energy  $\Delta E_{\text{int}}$ .<sup>c</sup> Percentage values: Relative contributions of the attractive pEDA terms  $\Delta E_{\text{elstat}}$  and  $\Delta E_{\text{orb}}$ .<sup>d</sup> Preparation energies of the molecule (M) and substrate (S) contain structural contributions and electronic excitations.<sup>e</sup> Deviations with respect to the PAW result are due to the basis set and simulation cell set-up differences.

## Pedestal

On the pristine surface, *pedestal* describes a mode that is also referred to as *tetra- $\sigma$*  mode. Here, acetylene or cyclooctyne adsorb between two dimers and form four C-Si bonds. This mode is however much less favorable than the DV-*pedestal* and therefore of no relevance for surface adsorption [9, 25]. Overall, the main difference of the *on-top* and *pedestal* modes is the interaction energy  $\Delta E_{\text{int}}$  which is about twice as large for the latter. This result is expected since four bonds instead of two are formed between molecule and surface. However,  $\Delta E_{\text{int}}$  is offset by excitation of the fragments into quintuplet states which is necessary to form four shared-electron C-Si bonds. Furthermore, the bond distance of the former acetylene  $\text{C}\equiv\text{C}$  triple bond is even significantly longer than a typical C-C single bond.

The pEDA can also provide an explanation for the reversed trend of bonding energy in the *pedestal* mode when comparing acetylene and cyclooctyne. The main contribution is given by steric repulsion of the bulkier cyclooctyne in the tight space provided by the DV. As a result, the difference in Pauli repulsion between acetylene and cyclooctyne ( $\Delta\Delta E_{\text{Pauli}}$ ) is increased slightly from 138 to 155 kJ/mol and  $\Delta\Delta E_{\text{orb}}$  rises significantly from 7 to 90 kJ/mol. The orbital interaction energies are reduced by 25-45 kJ/mol compared to acetylene. A smaller, albeit surprising, effect is the reduction of released RSE (-53 to -43 kJ/mol) which can be traced to the eight-membered ring also being strained at the position of the former triple bond. Its bond angles deviate by 7-10° from the ideal tetrahedral angle. This effect is somewhat offset by a larger dispersion attraction as cyclooctyne is positioned closer to the surface (-24 to -54 kJ/mol).

The origin of the large changes in  $\Delta\Delta E_{\text{orb}}$  term can be found by further dissecting it with the natural orbitals for chemical valence (NOCV) extension to the pEDA (Figure 6). Visual inspection of the deformation densities for acetylene shows that the four largest contributions of  $\alpha$ -spin

correspond to electron flow from the adsorbate (red) into the surface. In the  $\beta$ -spin channel, the flow of electrons is reversed (blue). These deformation densities correspond to the four C-Si shared-electron bonds formed from four unpaired electrons per fragment. Using the eigenvalues ( $\nu$ ) to quantify the amount of charge flow in the first four deformation densities, slightly polar (0.125  $e$ ) C-Si bonds in favor of C emerge, in line with the electronegativities of the elements. The triple bond is reduced to a single bond. Finally, the difference in  $\Delta E_{\text{orb}}$  between cyclooctyne (Figure 6, values in brackets) and acetylene is revealed to be caused by reduced charge flow into the molecule ( $\beta$ -spin). Here, the associated energy values for cyclooctyne are significantly lowered by about 30 kJ/mol per deformation density.

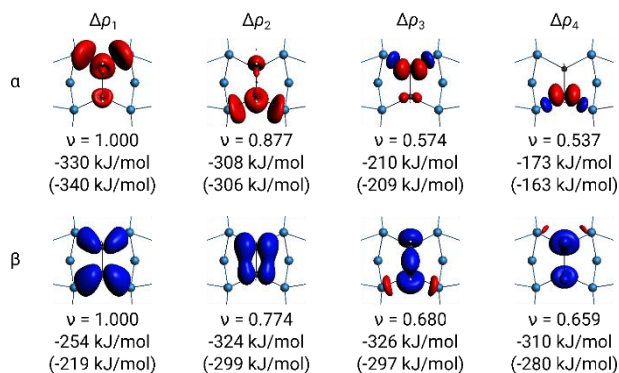


**Figure 6.** Most significant deformation densities  $\Delta\rho_n$ , eigenvalues ( $\nu$ ) and energies (total:  $\Delta E_{\text{orb}}(\alpha) = -1161$ ,  $\Delta E_{\text{orb}}(\beta) = -1313$ ) of acetylene in the *pedestal* mode. Corresponding energy values of cyclooctyne (total:  $\Delta E_{\text{orb}}(\alpha) = -1172$ ,  $\Delta E_{\text{orb}}(\beta) = -1212$ ) are given in brackets. Blue: charge accumulation, red: charge depletion. A quintuplet fragmentation was generated from the cleavage of four C-Si bonds. Orbitals in the Si-surface are often delocalized resulting in no deformation density being visible at the chosen iso value.

Side-on

The *side-on* mode shares characteristics with both other modes discussed above due to molecules being attached to one defect atom and one dimer atom. Consequently, the calculated pEDA terms fall in between *pedestal* and *on-top*. The reason for the relatively small adsorption energy can be found in a  $\Delta E_{\text{int}}$  term that is more comparable to *on-top*, while the surface preparation energy is more akin to *pedestal* even though triplet states are used instead of quintuplets. Furthermore, the newly described *side-on* mode is structurally similar to the *sub-surface* insertion mode (Figure S5) proposed from computations in the past for acetylene on pristine Si(001) [23]. Its formation is favored by -97 kJ/mol through a combination of increased electronic interaction and decreased preparation energy for the surface fragment. However, the bonding character is unaltered with electrostatic interaction amounting to roughly 40% in both cases.

### *Reaction networks*

In the last part of this study, the kinetic accessibility of different adsorption modes is discussed in addition to the already determined thermodynamic driving forces. We show here reaction networks generated from NEB calculations between reactants (pre-complexes) and adsorption modes discussed in the previous section. In two cases, this procedure leads to discovery of additional structures: for acetylene another *bridge* conformer (*bridge-E*) and for ethylene a *pedestal* variant that is only attached to two defect atoms (*pedestal-same*). Reaction barriers are calculated as the energy difference between a TS and the previous local minimum (i.e. intermediate). The reaction networks are more complex than on the pristine surface where acetylene adsorbs barrierless into the final state (*on-top*) [23] while for ethylene and cyclooctyne a short lived intermediate exists [11, 22, 26].

## Acetylene

In Figure 7, the reaction network of acetylene is found. Attempts to find the adsorption path (black arrows) into **1** did not converge via a single TS. Instead several minima appear on the reaction path corresponding to other already known adsorption modes. This behavior is somewhat expected since partial reduction of the C≡C bond coupled with simultaneous cleavage of two Si-Si bonds at the DV defect site requires a considerable activation energy which can be estimated from the preparation energy (862 kJ/mol). The *side-on* mode, on the other hand, is directly accessible (green arrows) but further reaction becomes unlikely when thermodynamic corrections are considered. Adsorption free energies ( $\Delta\Delta G_{\text{ads}}$ ) are dominated by the loss of translational and rotational entropy of the molecule and are therefore largely independent of adsorption mode. This change is estimated at 69 kJ/mol (*pedestal*) to 60 kJ/mol (*on-top*, [20]). Thus, the reaction traversing **TS1** is brought into competition with desorption and molecules in *side-on* are kinetically trapped at lower temperatures.

While the *bridge* mode (blue arrows) is rather stable, its transition state (**TS6**) is 30 kJ/mol higher than that of the *bridge-E* isomer (**TS4**). Furthermore, *E,Z*-isomerization is favored (**TS5** = 154 kJ/mol) over the barrier leading to *pedestal* (**TS3** = 192 kJ/mol). Thus, the path connecting both *bridge* modes (red arrows) with intermediate **II** emerges as the minimum energy pathway. The highest barrier in the pathway marked in red (**TS7**) amounts to 170 kJ/mol, which is in the same order of magnitude as other mode-conversion reactions (e.g. **TS1**, **TS3**). In summary, the acetylene + DV reaction network shows that adsorption into *side-on* is direct, while most other modes have small initial barriers. In contrast, paths between modes as well as into the thermodynamic sink (*pedestal*) require a larger activation energy.

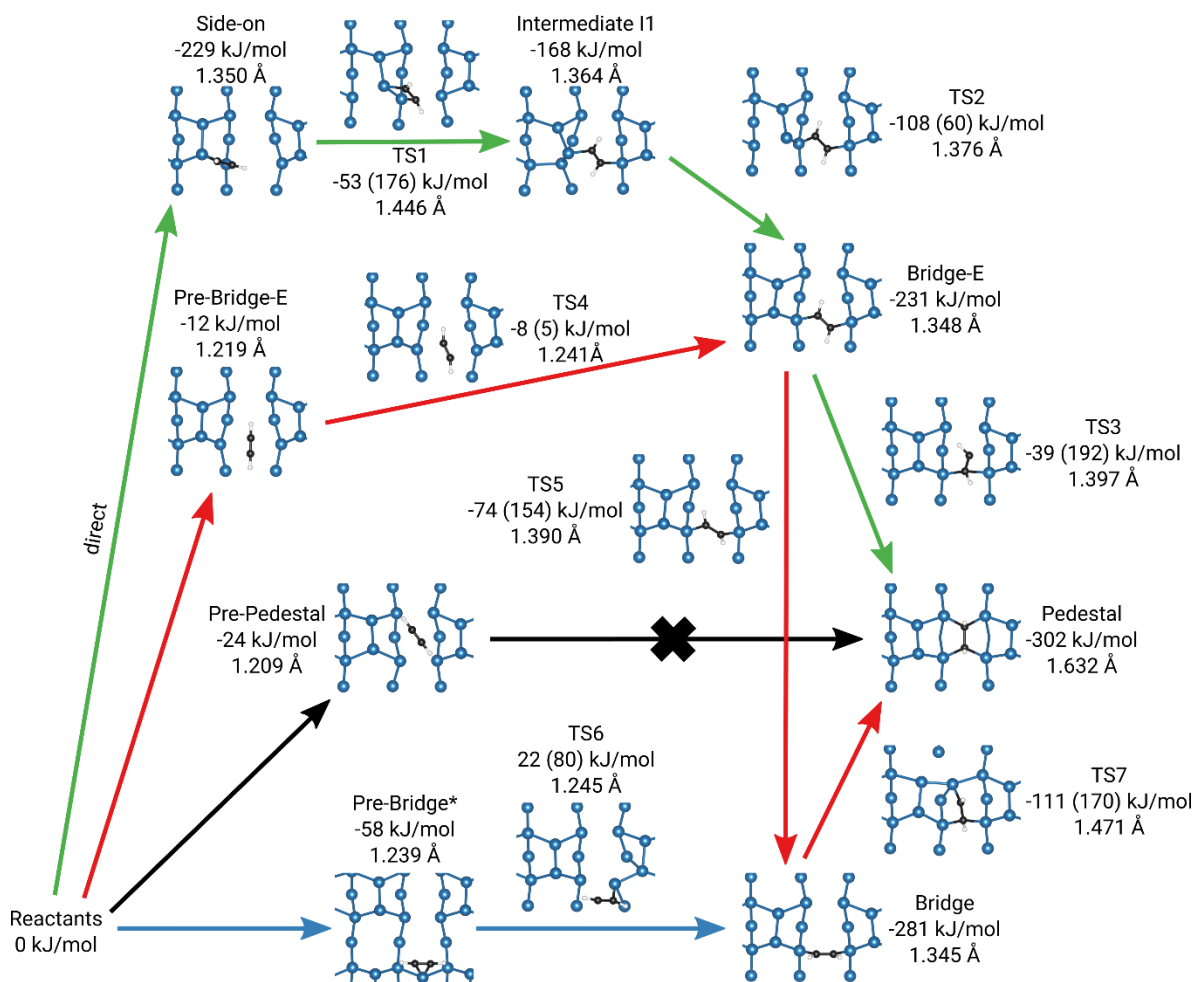


**Figure 7.** Reaction network of acetylene on the DV-defect. Energies are given relative to the isolated surface and molecule without thermodynamic corrections. Barriers are reported in parentheses and C-C bond lengths in Å. The major reaction path following the lowest transition states is highlighted in red. The pre-*bridge* structure (\*) is not a stable minimum but a TS between two *sub-surface* modes [23].

### Cyclooctyne

A reaction network has not been calculated for cyclooctyne. However, based on the analysis for acetylene and the adsorption energies computed (Table 2) some qualitative predictions can be made. Direct adsorption into the *pedestal* mode remains improbable even for the strained alkyne

since the preparation energy is not reduced sufficiently. In all other modes, RSE can be released which is expected to decrease initial adsorption barriers or remove them altogether. However, due to this additional stabilization, barriers between modes will likely be higher than for acetylene.

## Ethylene

In the case of ethylene, the reaction mechanism is similar for all pathways leading from the free molecule to the *pedestal* mode which is also the most stable structure here (Figure 8). Upon initial adsorption and independently of adsorption mode, two new C-Si connections are formed while the C=C bond is reduced to a single bond. Cleavage of the remaining C-C  $\sigma$ -bond is then facilitated by nucleophilic attack of a defect-Si atom. However, distance and angle of attack are generally constrained by the underlying substrate. The resulting high barriers make the final steps towards dissociation rate determining. Similar to acetylene, no direct adsorption of ethylene into the *pedestal* mode was found (black arrows). Of the initially accessible intermediates, *bridge* is the most stable with -190 kJ/mol. Further reaction towards the thermodynamic sink (blue arrows) requires overcoming a large barrier of 284 kJ/mol. The corresponding **TS13** is particularly unfavorable due to the occurrence of pentavalent Si. In contrast, the reaction paths running through the *side-on* (green arrows) and *pedestal-same* (red arrows) modes have barriers that are about 100 kJ/mol smaller. While a shorter C-C distance makes **TS10** (2.24 Å) more stable than **TS12** (2.40 Å) in absolute terms, all studied rate-determining saddle points have positive energies with respect to the free reactants. When considering Gibbs energies, TS energies become even more positive by 60 kJ/mol (*pedestal-same*) to 63 kJ/mol (*pedestal*) and therefore desorption of ethylene is kinetically increasingly favored at high temperatures. Since at low temperatures reactions will stop at their respective pre-dissociation intermediates (*side-on*, *pedestal-same*, *bridge*), adjustment

to the correct temperature range is critical for dissociating ethylene. However, under ultra-high vacuum conditions, equilibration between desorption and dissociation is expected to be slow. Therefore, ethylene is inferior to acetylene for saturating all defect atoms via the *pedestal* mode.

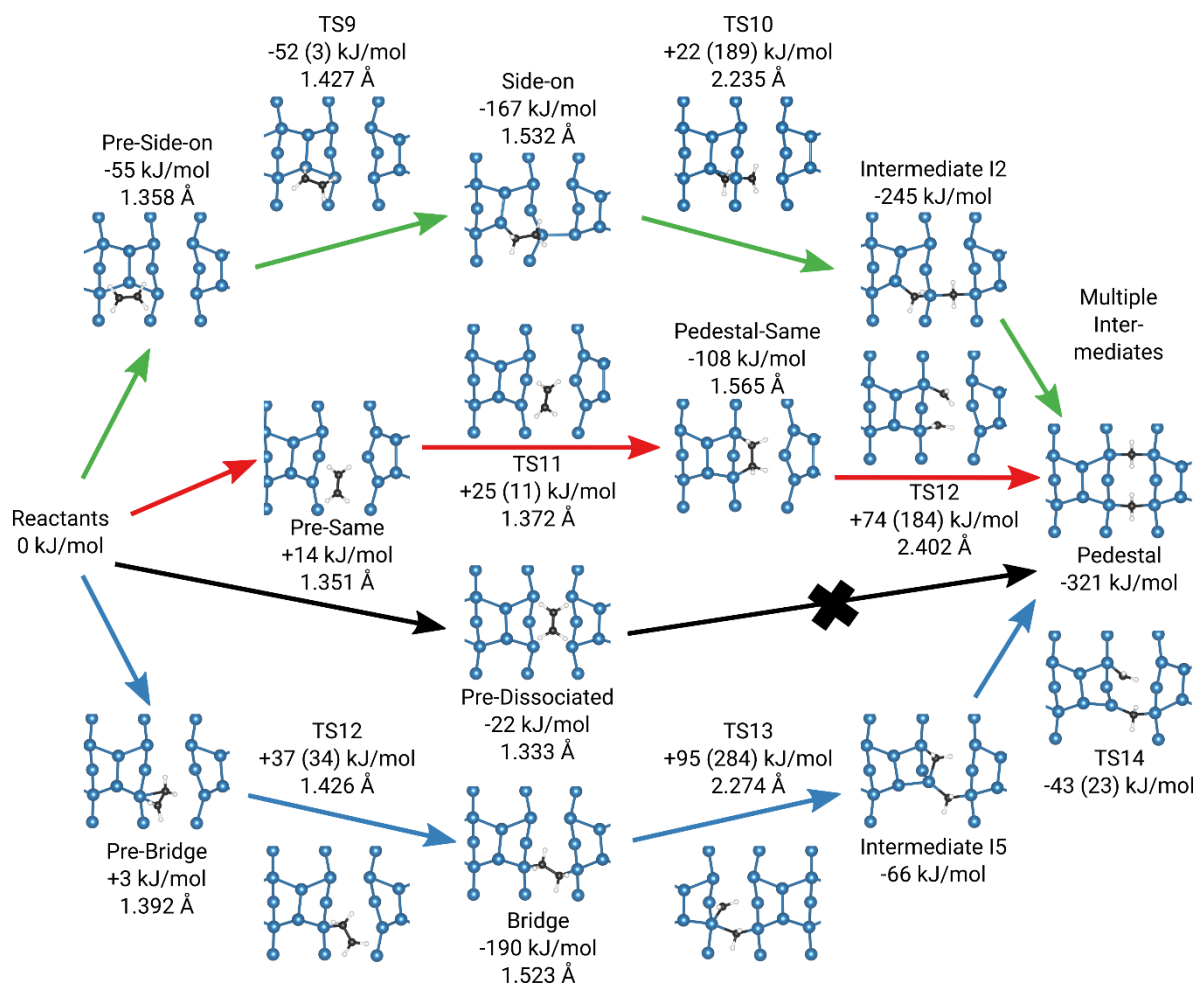


**Figure 8.** Reaction network of ethylene on the DV-defect. Electronic energies are given relative to the isolated surface and molecule. Barriers are given in parentheses and the central C-C bond length in Å. The reaction path following the lowest transition states is highlighted in red.

Apart from saturating the defect, cleavage of C=C double-bonds at semiconductor point defects could potentially have applications in heterogeneous catalysis. Thus, **TS12** situated between the *pedestal-same* and *pedestal* modes warrants further investigation.

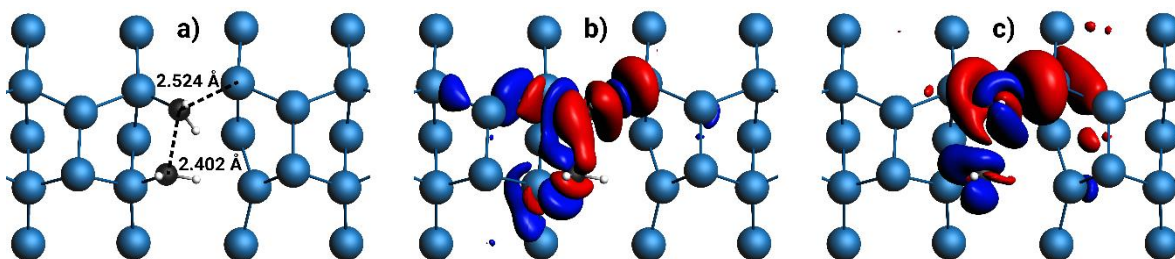


**Figure 9.** Analysis of **TS12**. (a) TS structure with selected bond lengths. (b)  $\Delta\rho(\alpha_3) = -78$  kJ/mol ( $\nu=0.432$ ,  $\text{iso}=0.0002$ ): Formation of the third C-Si bond. (c)  $\Delta\rho(\beta_3) = -83$  kJ/mol ( $\nu=0.446$ ,  $\text{iso}=0.0002$ ): Donation of density into the former C-C  $\sigma^*$ -bond. Not shown are  $\Delta\rho_1$  and  $\Delta\rho_2$  as they correspond to the two shared-electron C-Si bonds which are not of interest here.

In a previous study, we found a  $S_N2$ -type attack of Si(001) surface-dimer atoms to cleave an ether bond in tetrahydrofuran and diethylether [57]. There, an upcoming orbital contribution, as manifested in deformation densities, stabilizes the TS of the nucleophilic attack. For the present case, similar contributions can be found (Figure 9, Table S3). When decomposed by spin, formation of the new Si-C bond (Figure 9b) and weakening of the former C-C bond (Figure 9c) contribute about equally. The resulting barrier of C=C cleavage at the DV (184 kJ/mol) lies between unassisted (377 kJ/mol, experimental enthalpy [58]) and Fe-catalyzed (117 kJ/mol, B3LYP calculation [59]) dissociation energies in molecules. Thus, defects on semiconductor surfaces could play a role for catalytic cleavage of carbon-carbon bonds when questions like detaching the resulting fragments are solved.

## CONCLUSION

We show, in agreement with earlier results, that the bonded dimer vacancy where defect atoms form new single bonds is the most stable intrinsic point defect on Si(001). However, it is still accompanied by significant structural strain and the appearance of additional occupied bands in the band gap. These bands show low dispersion, suggesting reduced electron mobility with respect to the defect-free case. Reaction networks of unsaturated hydrocarbons, ethylene and acetylene as model adsorbates and cyclooctyne as interface building blocks, show much richer surface chemistry which is nevertheless limited to the defect itself. Neighboring dimers react in the same way as on the pristine surface. Surprisingly, we find the DV to be less reactive than the Si-dimer on the pristine surface. Barriers are only found towards adsorption modes incorporating defect atoms, such as *bridge* and *pedestal*. Those barriers, while small, likely appear as a result of absent dangling bonds. However, adsorption involving dimer atoms (*side-on*, *on-top*) is largely direct and can be stepwise transformed into the thermodynamically favored defect modes. Cyclooctyne shows larger steric hindrance in its reaction with the rather small defect cavity. On a more technical note, we show that isolated point defects require larger supercells and thicker slabs.

Thus, the DV exhibits a different reactivity than surrounding surface dimers. This fact might be used by molecules that selectively react with the surface dimers and not the defect. Subsequently deposited molecules which do react with the DV can then be used to introduce different desired functionalities already in the first ad-layer. Furthermore, this analysis of the electronic structure and reactivity of the surface defect can inspire more realistic computational models and thus helps developing new approaches for solving challenges encountered in organic functionalization of semiconductors and interface chemistry.

## ASSOCIATED CONTENT

### Supporting Information.

The supporting Information is available free of charge.

Converged slab-supercell of the dimer vacancy, benchmark of the partial Hessian approach, reconstructing a partial Hessian from fragment calculations, electronic structure of the flipped dimer, crystal orbitals of the pristine surface, hydrogen precovered surfaces, dispersion induced bending, *side-on* comparison to sublayer adsorption, pEDA of **TS12**, raw data archive. (PDF)

## AUTHOR INFORMATION

### Corresponding Author

\* ralf.tonner@chemie.uni-leipzig.de; Tel.: +49-341-97-36401

### Author Contributions

The manuscript was written through contributions of both authors. Both authors have given approval to the final version of the manuscript.

### Funding Sources

This research was funded by Deutsche Forschungsgemeinschaft (DFG) through SFB 1083 (grant number 223848855). Computational resources were provided by HLRS Stuttgart, CSC Frankfurt, HRZ Marburg and RZ Regensburg.

### Notes

The authors declare no conflict of interest.

## ACKNOWLEDGMENT

JNL thanks Fabian Pieck for helpful discussions.

## REFERENCES

1. Kumah, D. P.; Ngai, J. H.; Kornblum, L. Epitaxial Oxides on Semiconductors: From Fundamentals to New Devices. *Adv. Funct. Mater.* **2020**, *30*, 1901597.
2. Song, L.; Yu, X.; Yang, D. A review on graphene-silicon Schottky junction interface. *J. Alloys Compd.* **2019**, *806*, 63 – 70.
3. Loget, G. Water oxidation with inhomogeneous metal-silicon interfaces. *Curr. Opin. Colloid Interface Sci.* **2019**, *39*, 40 – 50.
4. Sundberg, P.; Karppinen, M. Organic and inorganic-organic thin film structures by molecular layer deposition: A review. *Beilstein J. Nanotechnol.* **2014**, *5*, 1104–1136.
5. Meng, X. An overview of molecular layer deposition for organic and organic-inorganic hybrid materials: mechanisms, growth characteristics, and promising applications. *J. Mater. Chem. A* **2017**, *5*, 18326–18378.
6. Zhou, H.; Bent, S. F. Molecular Layer Deposition of Functional Thin Films for Advanced Lithographic Patterning. *Appl. Mater. Interfaces* **2011**, *3*, 505–511.
7. Yoshinobu, J. Physical properties and chemical reactivity of the buckled dimer on Si(100). *Prog. Surf. Sci.* **2004**, *77*, 37 – 70.
8. Leftwich, T. R.; Teplyakov, A. V. Cycloaddition Reactions of Phenylazide and Benzylazide on a Si(100)-2×1 Surface. *J. Phys. Chem. C* **2008**, *112*, 4297–4303.

9. Pecher, J.; Schober, C.; Tonner, R. Chemisorption of a Strained but Flexible Molecule: Cyclooctyne on Si(001). *Chem. Eur. J* **2017**, *23*, 5459–5466.
10. Mette, G.; Dürr, M.; Bartholomäus, R.; Koert, U.; Höfer, U. Real-space adsorption studies of cyclooctyne on Si(001). *Chem. Phys. Lett.* **2013**, *556*, 70 – 76.
11. Länger, C.; Heep, J.; Nikodemiak, P.; Bohamud, T.; Kirsten, P.; Höfer, U.; Koert, U.; Dürr, M. Formation of Si/organic interfaces using alkyne-functionalized cyclooctynesprecursor-mediated adsorption of linear alkynes versus direct adsorption of cyclooctyne on Si(001). *J. Phys. Condens. Matter* **2018**, *31*, 034001.
12. Glaser, T.; Meinecke, J.; Länger, C.; Luy, J.-N.; Tonner, R.; Koert, U.; Dürr, M. Combined XPS and DFT investigation of the adsorption modes of methyl enol ether functionalized cyclooctyne on Si(001). *ChemPhysChem*, accepted, <https://doi.org/10.1002/cphc.202000870>.
13. Luy, J.-N.; Molla, M.; Pecher, L.; Tonner, R. Efficient hierarchical models for reactivity of organic layers on semiconductor surfaces. **2020**, DOI: 10.26434/chemrxiv.13342037.v1.
14. Raschke, M. B.; Höfer, U. Influence of steps and defects on the dissociative adsorption of molecular hydrogen on silicon surfaces. *Appl. Phys. B* **1999**, *68*, 649–655.
15. Mazzone, A. Acetylene adsorption onto Si(100): a study of adsorption dynamics and of surface steps. *Comput. Mater. Sci.* **2006**, *35*, 6 – 12.
16. Hata, K.; Kimura, T.; Ozawa, S.; Shigekawa, H. How to fabricate a defect free Si(001) surface. *J. Vac. Sci.* **2000**, *18*, 1933–1936.

17. Oh, S.-C.; Kim, K.-W.; Mamun, A. H.; Lee, H.-J.; Hahn, J. R. Role of coverage and vacancy defect in adsorption and desorption of benzene on Si(001)-2×n surface. *Bull. Korean Chem. Soc.* **2010**, *31*, 162–167.
18. Martin, J. A.; Savage, D. E.; Moritz, W.; Lagally, M. G. Structure, Stability, and Origin of (2×n) Phases on Si(100). *Phys. Rev. Lett.* **1986**, *56*, 1936–1939.
19. Mette, G.; Schwalb, C.; Dürr, M.; Höfer, U. Site-selective reactivity of ethylene on clean and hydrogen precovered Si(001). *Chemical Physics Letters* **2009**, *483*, 209 – 213.
20. Pecher, J.; Mette, G.; Dürr, M.; Tonner, R. Site-Specific Reactivity of Ethylene at Distorted Dangling-Bond Configurations on Si(001). *ChemPhysChem* **2017**, *18*, 357–365.
21. Sorescu, D. C.; Jordan, K. D. Theoretical Study of the Adsorption of Acetylene on the Si(001) Surface. *J. Phys. Chem. B* **2000**, *104*, 8259–8267.
22. Pecher, J.; Tonner, R. Precursor States of Organic Adsorbates on Semiconductor Surfaces are Chemisorbed and Immobile. *ChemPhysChem* **2017**, *18*, 34–38.
23. Pecher, L.; Tonner, R. Bond Insertion at Distorted Si(001) Subsurface Atoms. *Inorganics* **2018**, *6*, 17.
24. Cho, J.-H.; Kleinman, L. Adsorption kinetics of acetylene and ethylene on Si(001). *Phys. Rev. B* **2004**, *69*, 075303.
25. Miotto, R.; Ferraz, A. C.; Srivastava, G. P. Acetylene adsorption on the Si(001) surface. *Phys. Rev. B* **2002**, *65*, 075401.

26. Pecher, L.; Schmidt, S.; Tonner, R. Modeling the Complex Adsorption Dynamics of Large Organic Molecules: Cyclooctyne on Si(001). *J. Phys. Chem. C* **2017**, *121*, 26840–26850.
27. Agard, N. J.; Prescher, J. A.; Bertozzi, C. R. A Strain-Promoted [3 + 2] Azide-Alkyne Cycloaddition for Covalent Modification of Biomolecules in Living Systems. *J. Am. Chem. Soc.* **2004**, *126*, 15046–15047.
28. Münster, N.; Nikodemiak, P.; Koert, U. Chemoselective Layer-by-Layer Approach Utilizing Click Reactions with Ethynylcyclooctynes and Diazides. *Org. Lett.* **2016**, *18*, 4296–4299.
29. Roberts, N.; Needs, R. J. Total energy calculations of missing dimer reconstructions on the silicon (001) surface. *J. Phys. Condens. Matter.* **1989**, *1*, 3139–3143.
30. Kirichenko, T. A.; Banerjee, S. K.; Hwang, G. S. Interaction of neutral vacancies and interstitials with the Si(001) surface. *Phys. Rev. B* **2004**, *70*, 045321.
31. Wang, J.; Arias, T. A.; Joannopoulos, J. D. Dimer vacancies and dimer-vacancy complexes on the Si(100) surface. *Phys. Rev. B* **1993**, *47*, 10497–10508.
32. Fu, C.-C.; Weissmann, M.; Saul, A. Diffusion pathways for Si ad-dimers on Si(001): a high temperature molecular dynamics study. *Surf. Sci.* **2001**, *481*, 97 – 104.
33. Owen, J.; Bowler, D.; Goringe, C.; Miki, K.; Briggs, G. Identification of the Si(001) missing dimer defect structure by low bias voltage STM and LDA modelling. *Surf. Sci.* **1995**, *341*, L1042 – L1047.

34. Sueoka, K.; Kamiyama, E.; Spiewak, P.; Vanhellefont, J. Review Properties of Intrinsic Point Defects in Si and Ge Assessed by Density Functional Theory. *ECS J. Solid State Sci. Technol.* **2016**, *5*, P3176–P3195.
35. Kirichenko, T. A.; Banerjee, S. K.; Hwang, G. S. Mechanisms of monovacancy annihilation and type-A defect creation on Si(001)-2×1. *Surf. Sci.* **2004**, *555*, 187 – 192.
36. Hamers, R. J.; Köhler, U. K. Determination of the local electronic structure of atomic sized defects on Si(001) by tunneling spectroscopy. *J. Vac. Sci.* **1989**, *7*, 2854–2859.
37. Yu, S.-Y.; Kim, H.; Koo, J.-Y. Extrinsic Nature of Point Defects on the Si(001) Surface: Dissociated Water Molecules. *Phys. Rev. Lett.* **2008**, *100*, 036107.
38. Okano, S.; Oshiyama, A. A new alternative model of type-C defects on Si(100) surfaces. *Surf. Sci.* **2004**, *554*, 272 – 279.
39. Kresse, G.; Hafner, J. Ab initio molecular dynamics for liquid metals. *Phys. Rev. B* **1993**, *47*, 558.
40. Kresse, G.; Furthmüller, J. Efficiency of ab-initio total energy calculations for metals and semiconductors using a plane-wave basis set. *Comput. Mater. Sci.* **1996**, *6*, 15.
41. Kresse, G.; Furthmüller, J. Efficient iterative schemes for ab initio total-energy calculations using a plane-wave basis set. *Phys. Rev. B* **1996**, *54*, 11169–11186.
42. Perdew, J. P.; Burke, K.; Ernzerhof, M. Generalized Gradient Approximation Made Simple. *Phys. Rev. Lett.* **1996**, *77*, 3865–3868.

43. Kresse, G.; Joubert, D. From ultrasoft pseudopotentials to the projector augmented-wave method. *Phys. Rev. B* **1999**, *59*, 1758–1775.
44. Grimme, S.; Antony, J.; Ehrlich, S.; Krieg, H. A consistent and accurate ab initio parametrization of density functional dispersion correction (DFT-D) for the 94 elements H-Pu. *J. Chem. Phys* **2010**, *132*, 154104.
45. Grimme, S.; Ehrlich, S.; Goerigk, L. Effect of the damping function in dispersion corrected density functional theory. *J. Comput. Chem.* **2011**, *32*, 1456–1465.
46. Boyd, D. R. J. Infrared Spectrum of Trideuterosilane and the Structure of the Silane Molecule. *J. Chem. Phys* **1955**, *23*, 922–926.
47. Henkelman, G.; Uberuaga, B. P.; Jónsson, H. A climbing image nudged elastic band method for finding saddle points and minimum energy paths. *J. Chem. Phys* **2000**, *113*, 9901–9904.
48. Henkelman, G.; Jónsson, H. A dimer method for finding saddle points on high dimensional potential surfaces using only first derivatives. *J. Chem. Phys* **1999**, *111*, 7010–7022.
49. Raupach, M.; Tonner, R. A periodic energy decomposition analysis method for the investigation of chemical bonding in extended systems. *J. Chem. Phys.* **2015**, *142*, 194105.
50. BAND2019, SCM, Theoretical Chemistry, Vrije Universiteit, Amsterdam, The Netherlands, <http://www.scm.com>, accessed 08.01.2021.
51. Van Lenthe, E.; Baerends, E. J. Optimized Slater-type basis sets for the elements 1-118. *J. Comput. Chem.* **2003**, *24*, 1142–1156.

52. Philipsen, P. H. T.; van Lenthe, E.; Snijders, J. G.; Baerends, E. J. Relativistic calculations on the adsorption of CO on the (111) surfaces of Ni, Pd, and Pt within the zeroth-order regular approximation. *Phys. Rev. B* **1997**, *56*, 13556–13562.
53. Bondi, A. van der Waals Volumes and Radii. *The Journal of Physical Chemistry* **1964**, *68*, 441–451.
54. Okada, H.; Fujimoto, Y.; Endo, K.; Hirose, K.; Mori, Y. Detailed analysis of scanning tunneling microscopy images of the Si(001) reconstructed surface with buckled dimers. *Phys. Rev. B* **2001**, *63*, 195324.
55. Pecher, L.; Schmidt, S.; Tonner, R. Dispersion-mediated steering of organic adsorbates on a precovered silicon surface. *Beilstein J. Org. Chem.* **2018**, *14*, 2715–2721.
56. Zhu, X. Y.; Huang, X. J. SiH<sub>2</sub> adsorption on the single dimer vacancy of the Si(100) surface. *J. Phys. Condens. Matter.* **2006**, *18*, 7045–7050.
57. Pecher, L.; Laref, S.; Raupach, M.; Tonner, R. Ethers on Si(001): A Prime Example for the Common Ground between Surf. Sci. and Molecular Organic Chemistry. *Angew. Chem. Int. Ed.* **2017**, *56*, 15150–15154.
58. Blanksby, S. J.; Ellison, G. B. Bond Dissociation Energies of Organic Molecules. *Acc. Chem. Res.* **2003**, *36*, 255–263.
59. Holthausen, M. C.; Fiedler, A.; Schwarz, H.; Koch, W. How Does Fe<sup>+</sup> Activate C-C and C-H Bonds in Ethane? A Theoretical Investigation Using Density Functional Theory. *J. Phys. Chem.* **1996**, *100*, 6236–6242.